PROCEEDINGS OF SCIENCE

Standard Model and Heavy Ion Physics from ATLAS and CMS

Elisabetta Gallo[*†]
DESY and University of Hamburg
E-mail: gallo@mail.desy.de

Recent highlights on standard model results from the ATLAS and CMS Collaborations at the LHC are presented. The results cover W and Z physics, top quark production and jets cross sections. Heavy ions results obtained recently by the CMS Collaboration are reviewed.

55th International Winter Meeting on Nuclear Physics
23-27 January, 2017
Bormio, Italy

[*]Speaker.
[†]On behalf of the ATLAS and CMS Collaborations

© Copyright owned by the author(s) under the terms of the Creative Commons Attribution-NonCommercial-NoDerivatives 4.0 International License (CC BY-NC-ND 4.0).

PoS(BORMIO2017)042

1. Introduction

The ATLAS and CMS Collaborations at the LHC are providing a wealth of physics results in tests of the electroweak (EW) and strong interactions. The increased precision in the measurements is accompanied by the more and more accurate calculations in perturbative QCD (pQCD) achieved in the last years, showing the interest of the theoretical community. The data from Run 1 represent a well understood dataset and highlights from the latest publications are reviewed here. The Run 2 data open a new regime in centre-of-mass (c.m.) energy with a much increased luminosity and some of the preliminary results are reported.

The LHC had a fantastic performance in 2016, exceeding expectations, reaching an instantaneous luminosity of 1.5×10^{34} cm^{-2}sec^{-1} and a peak efficiency of 58%. The ATLAS and CMS experiments collected data with more than 92% efficiency and approximately 36 fb^{-1} of integrated luminosity were collected for physics (Fig. 1). The high instantaneous luminosity comes at the price of pileup, the number of overlapping proton-proton interactions in one bunch crossing (Fig. 1). In 2016 an average of 24 pileup interactions was observed. However the experiments have developped tools to mitigate the effect of pileup at the trigger and object reconstruction level. This is shown for instance in Fig. 1 for single electron triggers at the High Level Trigger (HLT), in the CMS barrel calorimeter. The trigger efficiency, derived here from the data for different thresholds and selection criteria, shows almost no dependence on the number of interactions.

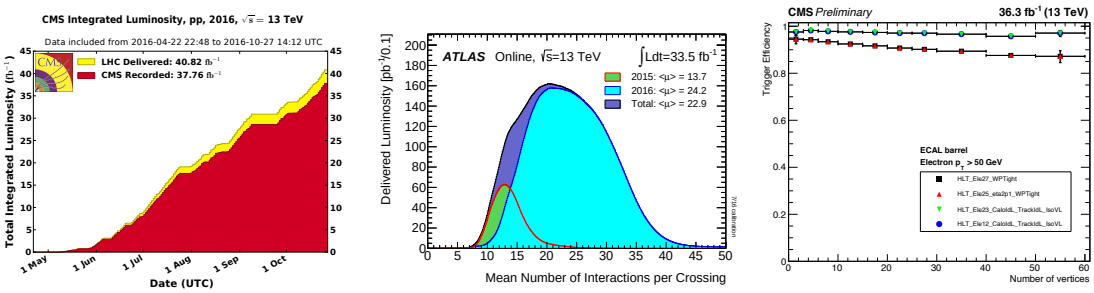

Figure 1: From the left to the right: CMS integrated luminosity in 2016; number of interactions in one bunch crossing in ATLAS in 2015-2016; trigger efficiency for electrons at the HLT in the CMS barrel electromagnetic calorimeter, for different thresholds and criteria and as a function of the number of vertices.

In the following some recent highlights on EW and QCD results are reported, from recent publications on Run 1 data and from first Run 2 results. Additional details on jets at ATLAS can be found in [1]. Heavy ions results from CMS are reported in the second part of these proceedings, while heavy ions results from ATLAS are summarized in [2]. The ATLAS and CMS detectors are described in [3, 4].

2. Standard Model Results

A compact summary plot of cross sections for standard model (SM) processes at ATLAS is shown in Fig. 2. The plot shows cross sections for the main processes, from production of W and Z, to Higgs and diboson production, at the three c.m. energies of 7, 8 amd 13 TeV. The theory

PoS(BORMIO2017)042

curves, shown with their uncertainty (grey) bands, are by now calculated beyond next-to-next-leading order (NNLO) for many processes. The agreement between the experimental measurement and the theory over many orders of magnitude is remarkable.

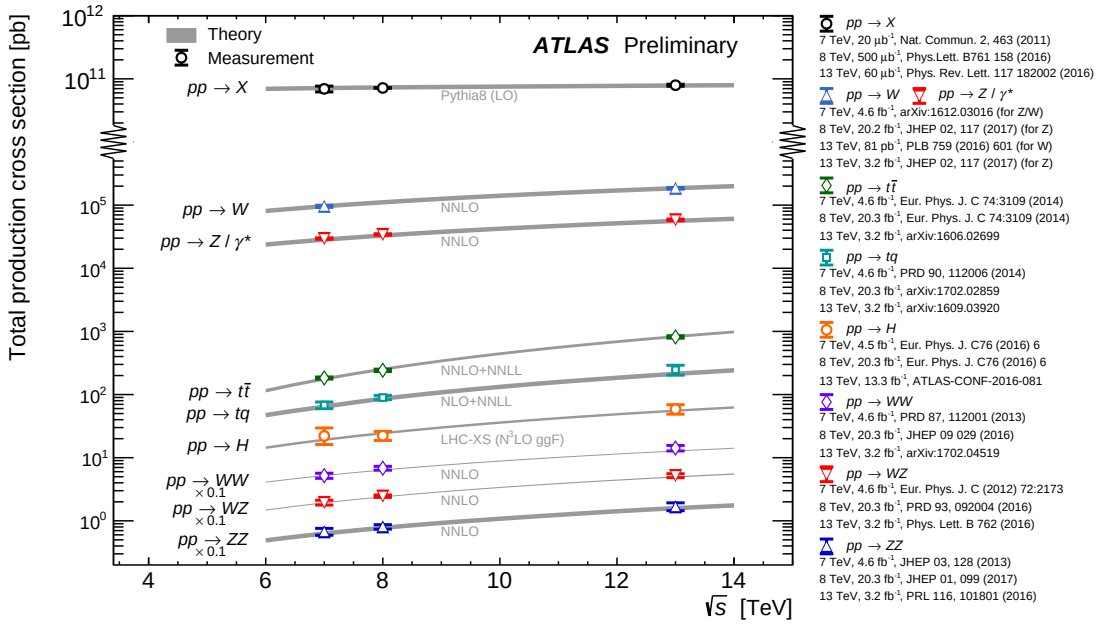

Figure 2: Summary of production cross-section measurements by ATLAS, presented as a function of centre-of-mass energy for few selected SM processes. The diboson cross sections are scaled by a factor 0.1 for clarity.

2.1 Precision Measurement of the W and Z Cross Sections and of m_W at ATLAS

The ATLAS Collaboration has presented a new precise measurement of W and Z/γ^* cross sections, using data collected in 2011 at $\sqrt{s} = 7$ TeV, corresponding to 4.6 fb^{-1} of integrated luminosity [8]. The measurement is based on approximately 15M W decays and 1.6M Z decays, in the electron and muon channels combined in a common fiducial phase space, taking into account the correlated uncertainties. Systematic uncertainties are 0.6% for the total fiducial W cross section and $< 0.32\%$ for the Z cross section. The luminosity uncertainty for that period is 1.8%, it however cancels out in ratios. Figure 3 shows the ratio of W^+/W^- and W/Z cross sections in the fiducial region of the selection. The results are compared to theoretical predictions at NNLO in QCD, calculated using the programs DYNNLO 1.5 [14] and FEWZ 3.1.b2 [15] and including EW corrections at NLO. The calculation is shown with various parametrizations of the proton parton density (PDF) functions. While the ratio W^+/W^- is well reproduced, the theory with different PDFs predict a ratio W/Z which is in tension with the data. The comparison of the prediction to the differential distributions (Fig. 3) poses an additional challenge. A QCD analysis of the data seems to indicate an increased contribution of the strange-quark sea distribution, compared to that of present PDF parametrizations.

Using the same data sample, ATLAS performed the first measurement of the W mass at the LHC [6]. In hadron colliders the mass of the W boson can be extracted from the Jacobian edge

PoS(BORMIO2017)042

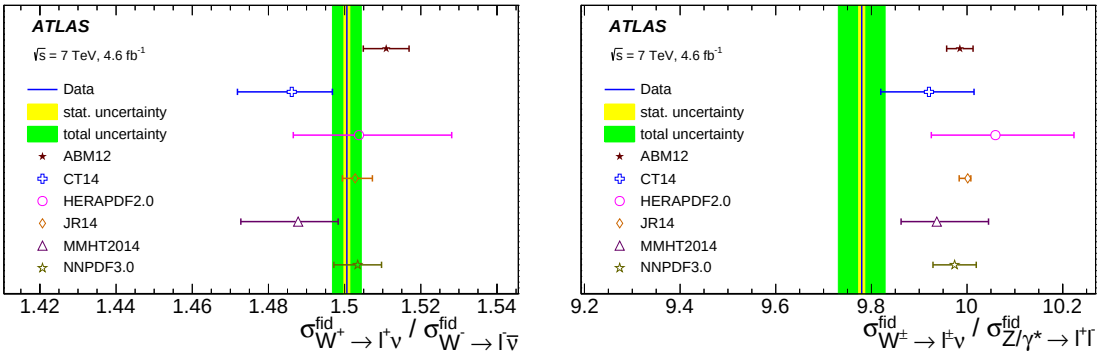

Figure 3: Ratio of the fiducial cross sections W^+/W^- and W/Z as measured by ATLAS with the 2011 data at $\sqrt{s}$=7 TeV. The measurement (solid blue line, shown with the statistical uncertainty as yellow band, and total uncertainty as green band) is compared to the theoretical prediction with different proton PDFs and relative PDF uncertainty (symbols, with error bars).

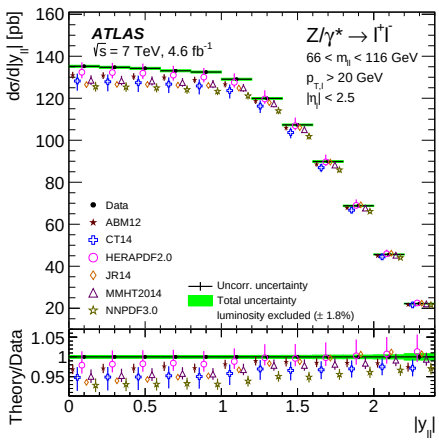

Figure 4: Differential cross-section measurement by ATLAS for the Drell-Yan process $Z\gamma^* \to ll$, as a function of the dilepton rapidity, in the central rapidity region and for $66 < m_{ll} < 116$ GeV. In this mass range the total uncertainty per bin is $< 0.5\%$. The data are compared to calculations at NNLO in QCD and with NLO EW corrections. The predictions are shown as open points with error bars corresponding to the statistical+PDF uncertainty, with various PDFs and displaced in each bin for better visibility. The lower part shows the ratios between theory and data.

of the decay $W \to l\nu$, where l is here either a muon or an electron. Variables which are sensitive are the transverse mass (m_T) and the transverse momentum of the lepton (p_T^l). Templates of the expected final state distributions for these two variables were simulated for several values of m_W and then fitted to the data to extract the measured value. The two kinematic distributions require perfect modelling, which was achieved by ATLAS thanks to an excellent understanding of the leptons (calibration and efficiency), of the recoil and of the missing transverse energy, and of the theoretical contributions as reported above. Events with two muons or two electrons from Z decays play an important role, as they are used to check calibration and performance. The W mass is extracted separately for W^+/W^-, for the two electron and muon channels and for the two kinematic

PoS(BORMIO2017)042

distributions, and then combined, resulting in

$$m_W = 80369.6 \pm 6.8(\text{stat.}) \pm 10.6(\text{exp. sys.}) \pm 13.6(\text{mod. syst.})\text{MeV} \quad (2.1)$$

$$m_W = 80369.5 \pm 18.5\text{MeV} \quad (2.2)$$

where the first uncertainty is statistical, the second one corresponds to the experimental systematic uncertainties and the last one to physics modelling. This last one is dominating and can be only reduced in future with better knowledge of PDFs and improved predictions of W and also Z cross sections. The result is compared to other measurements at colliders in Fig. 5, showing that it is in good agreement and very competitive. Electroweak radiative corrections in the SM give a relation between the W, top and Higgs boson masses, as shown in Fig. 5. Here the top mass $m_t = 172.84 \pm 0.70$ GeV is taken from the latest ATLAS determination, and the Higgs mass $m_H = 125.09 \pm 0.24$ GeV is the Run 1 legacy ATLAS and CMS combined result. The 68% and 95% contours show that all results come well together and strengthen the verification of the standard model.

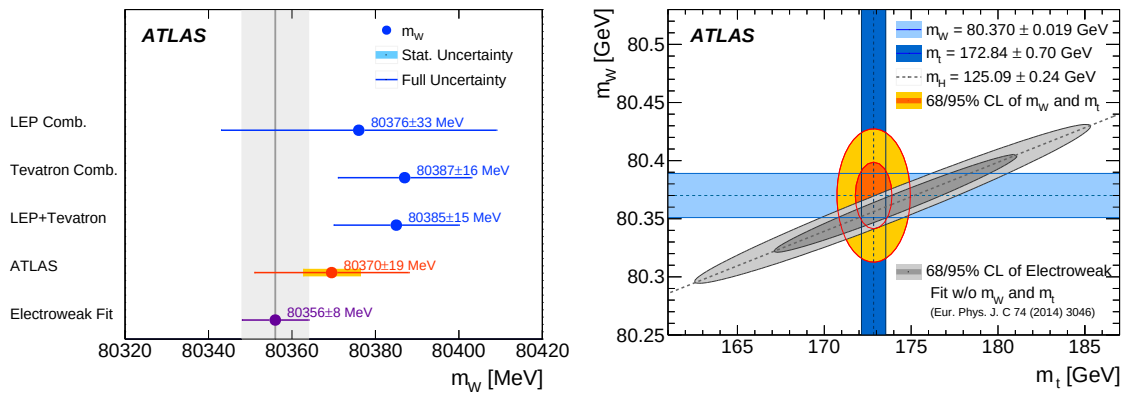

Figure 5: ATLAS measurement for the W mass compared (left plot) to previous results at other colliders and to the EW fits, with top mass and Higgs boson mass values as described in the text. The 68% and 95% confidence level contours of the EW fits are shown on top of the measurements in the right figure.

2.2 Diboson Production

The high c.m. energy at the LHC and the steadily increasing luminosity allow ATLAS and CMS a detailed study of VV final states, where V=W,Z,γ. Not only this is a test of the SM, including tests of the non-Abelian nature of the EW theory, but diboson events are background to Higgs production and to searches for new resonances decaying into two bosons, and a testing ground for anomalous triple gauge couplings (aTGCs). Cross sections for ZZ and WZ production have been determined at all three c.m. energies and compared to the very recent NNLO calculations available [7]. Figure 6 shows the WZ [8, 9] and ZZ [10, 11] cross sections as a function of the c.m. energies for ATLAS and CMS, compared to the NLO and NNLO theory predictions. The measurements are performed in the decays to electrons or muons in a fiducial region. They are then extrapolated to the total phase space in order to compare the two experiments' results to the

PoS(BORMIO2017)042

theory, as shown in Fig. 6 in the mass region $60 < m_{ll} < 120$ GeV for the Z decay leptons. The measurements are in agreement with the SM and they are still dominated by the statistics of the samples, therefore these analyses will profit a lot from the increasing luminosity.

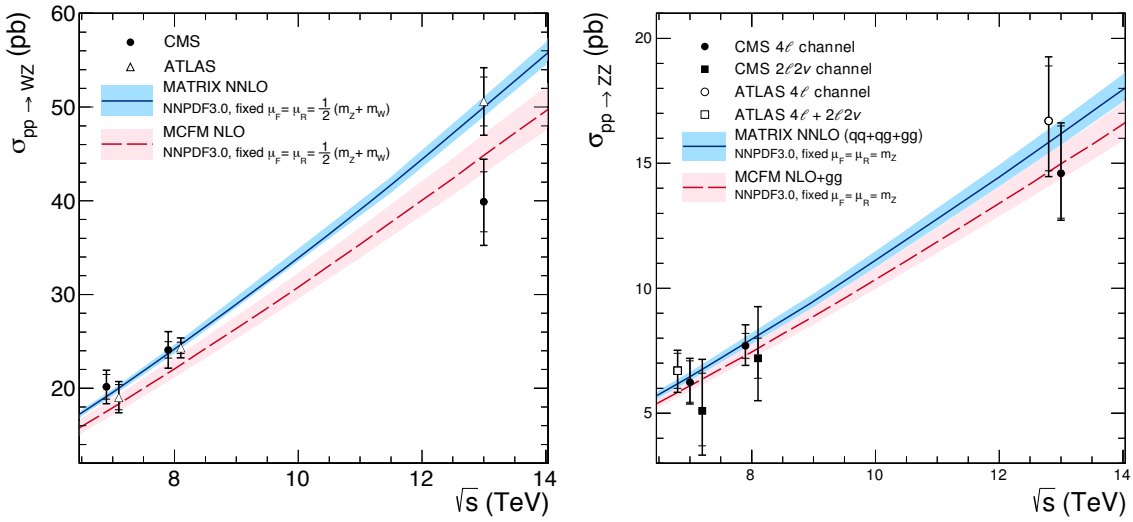

Figure 6: ATLAS and CMS measurements for the WZ and ZZ cross sections extrapolated to the total phase space and compared to NLO and NNLO QCD calculations.

2.3 Top

The LHC is a top factory and the measurement of the top cross section was one of the first measurements published with the Run 2 data, using the dilepton channel, where the two W's from the top decay in either a muon or an electron. By now the cross section at $\sqrt{s} = 13$ TeV is measured also in the so-called lepton+jets channel, in which one of the W decays leptonically and the second one hadronically. The total cross section at the three c.m. energies of 7, 8 and 13 TeV is shown in Fig. 7. The inset displays a zoom on the c.m. energy of 13 TeV, showing the perfect agreement among the different measurements and with the prediction. The most precise measurement is at the moment of writing the CMS result in the l+jets channel [12] with the 2015 data:

$$\sigma_{t\bar{t}} = 835 \pm 3(\text{stat.}) \pm 23(\text{syst.}) \pm 23(\text{lumi}) \text{ pb} \tag{2.3}$$

with an overall uncertainty of 4%. The differential cross section in the same l+jets channel as a function of the p_T of the top quark is displayed in Fig. 7 in comparison to MC models and different theoretical calculations (see references in [12]), including to a full NNLO calculation. The cross section is unfolded back to the parton level, with uncertainties dominated on the experimental side by the jet energy scale, on the theoretical side by the parton showers and hadronization corrections. The lower part of the right figure shows the ratio with the data. A longstanding issue in Run 1 was the steeper spectrum in MC compared to data for $p_t \geq 200$ GeV. This result shows that including higher orders brings the calculation in better agreement with the data inside the uncertainties.

PoS(BORMIO2017)042

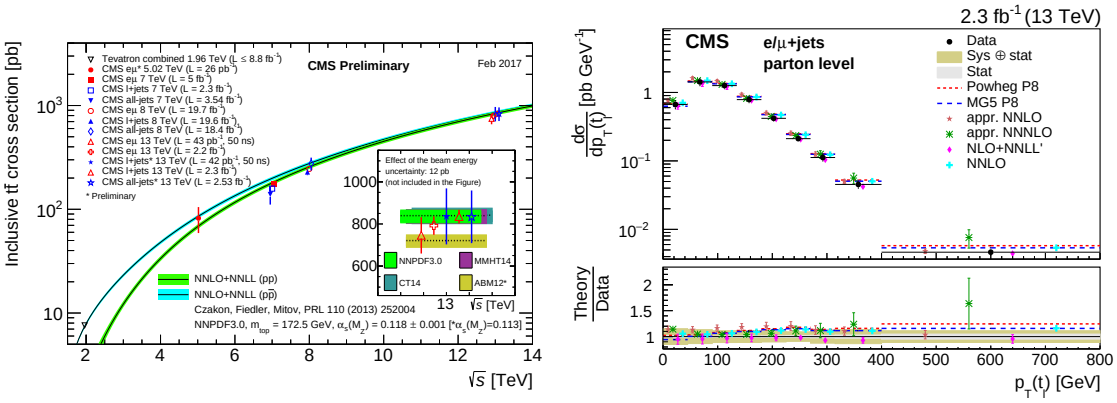

Figure 7: Left: Total cross section for top production at ATLAS and CMS, as a function of the c.m. energy. The data are plotted in comparison to the NNLO+NNLL theory calculation from Czakon et al., as referenced in the figure. Right: Differential cross section as a function of the p_T of the top, measured by CMS and in comparison to various MC models and calculations.

2.4 QCD Jets and Measurement of α_S

Jet cross sections are a way to test pQCD, are sensitive to parton densities and can be used to extract the strong coupling constant α_S. CMS has recently published a very precise measurement of double differential cross sections in jets p_T and rapidity y [13] at $\sqrt{s} = 8$ TeV. Jets were reconstructed with the anti-k_T clustering algorithm with a size parameter of 0.7, and in large phase-space region covering p_T from 74 GeV up to 2.5 TeV and jet absolute rapidity up to $|y| = 3$. A special low p_T pileup run with limited luminosity allowed to collect additional jets data in the region up to $|y| = 4.7$. The differential cross sections are shown in Fig. 8 corrected to the hadron level. They are compared to a pQCD prediction at NLO calculated by using the NLOJet++ [16] program as implemented in FASTNLO [17]. The prediction is shown with the CT10 PDF parametrization, and is corrected for non perturbative (NP) effects and for EW corrections (this last correction only in the high p_T region). Data and theory agree over several orders of magnitude, confirming the success of pQCD. These data have sensitivity to PDFs and can be used to constrain further the parton densities and especially the gluon.

The high-p_T jet bins were used to extract the value of α_S, by fitting the NLO prediction, which depends on α_S, to the data differential cross sections taking into account the correlations between the bins. The best fit value is:

$$\alpha_S(M_Z)(NLO) = 0.1164^{+0.0025}_{-0.0029}(\text{PDF})^{+0.0053}_{-0.0028}(\text{scale}) \pm 0.0001(\text{NP})^{+0.0014}_{-0.0015}(\text{exp.}) \quad (2.4)$$

$$= 0.1164^{+0.0060}_{-0.0043} \quad (2.5)$$

where the scale uncertainty refers to higher order corrections, NP to non-perturbative corrections and the experimental uncertainties are dominated by the jet energy scale. The high p_T region was divided in 9 bins and the value of α_S was extracted from a fit in each bin, in order to check the dependence on the scale Q. The Q scale in each bin in p_T is evaluated as the cross section weighted average p_T in that range. The extracted values of $\alpha_s(M_Z)$ are evolved to the corresponding Q scale in that range using the 2-loop 5-flavour renomalization group evolution equation. The resulting

PoS(BORMIO2017)042

Collisions	c.m. energy	Integrated luminosity
p-p	5 TeV	30 pb^{-1}
Pb-Pb	5 TeV	0.5 nb^{-1}
p-Pb (2016)	8 TeV	190 nb^{-1}
Pb-Pb (2016)	5 TeV	0.5 nb^{-1}

Table 1: Heavy ions runs in Run 2 with c.m. energies and approximate integrated luminosities useful for physics, collected by the CMS experiment.

$\alpha_S(Q)$ points are displayed as black dots in Fig. 8 over the wide energy scale range between 86 GeV and 1.5 TeV, showing the running of the strong coupling constant inside the CMS data alone.

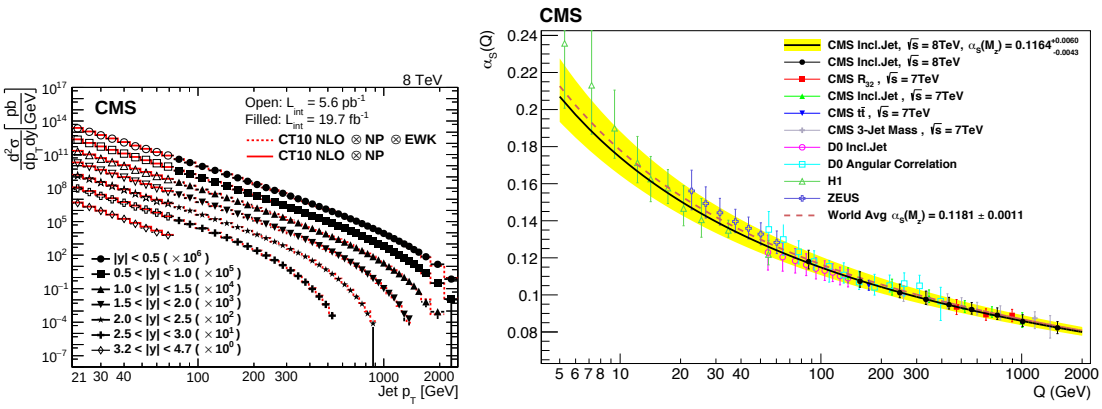

Figure 8: Left: Double differential jet cross sections measured by CMS at $\sqrt{s} = 8$ TeV, as a function of jet p_T and y. The open and full points refer to different data samples at low and high p_T, respectively. The pQCD NLO calculation was calculated by using the NLOJet++ as implemented in FASTNLO. Right: The strong coupling constant α_S as a function of the scale Q from various experiments. The solid line is the measured CMS value with the uncertainties, the black dots show the nine p_T bins. The dashed line is the world average. The curves are obtained by evolving $\alpha_S(M_Z)$ using the 2-loop 5-flavour renormalization group equation.

3. Heavy Ions Results at CMS

Heavy ions collisions provide another testing ground for QCD, in extreme conditions of very high temperature and very high density of particles. Experiments at the Relativistic Heavy Ion Collider (RHIC) have established in nucleus-nucleus interactions the formation of a state of matter with deconfined quarks and gluons, known as Quark-Gluon Plasma (QGP). The temperature of the medium depends on the collision energy and the LHC is providing many additional studies at higher $\sqrt{s_{NN}}$. Here some of the latest highlights from CMS are reported. Table 1 reports the heavy ions runs and respective integrated luminosities until the 2016 run. The collisions between lead-lead ions are cross-checked with collisions with proton-lead and proton-proton collisions at the same c.m. energies.

PoS(BORMIO2017)042

One of the properties of the QGP is its opaqueness to high-energy partons, which manifests itself in the suppression of hard probes (J/ψ, Υ, jets, high p_T particles). Hard-scattered partons are expected to loose energy as they traverse the QGP via elastic collisions and medium-induced gluon radiation. This effect has been observed as "jet quenching", where in two-jet events one of the high p_T jet looses energy while traversing the medium and therefore there is an imbalance in the transverse momentum of the two jets; or in a suppression of the J/ψ yield in lead-lead compared to pp collisions. It is quantified by measuring the nuclear modification factor R_{AA}, which is the ratio of the final-state probe yields at a given p_T, to that expected for pp collisions in absence of the medium:

$$R_{AA} = \frac{dN_{AA}/dp_T}{< N_{coll} > dN_{pp}dp_T}, \tag{3.1}$$

where $< N_{coll} >$ is the average number of binary nucleon-nucleon collisions.

A second property of the medium is the azimuthal anisotropy of hadrons, causing long-range two-particle correlations at large relative pseudorapidity, also already observed at RHIC. A key signature of these correlations is an enhanced structure on the near side ($|\Delta\phi| \simeq 0$) of two-particle $\Delta\phi - \Delta\eta$ correlations that extends up to very high rapidity, $|\Delta\eta| \simeq 4$, the so-called "ridge". The first evidence for a ridge at the LHC was actually reported in 2010 in high multiplicity events in pp collisions by CMS [18]. The ridge is by now extensively studied at the LHC and it has been suggested that the hydrodynamic collective flow of the strongly interacting medium is responsible for these long-range correlations in heavy ions collisions. The azimuthal correlation structure of the final state hadrons is usually described in terms of its Fourier components, where the second (elliptic or v_2) and third (triangular or v_3) components reflect the medium response to the initial collisions geometry and its fluctuations, respectively.

CMS is particularly suited for studies of heavy ions collisions, thanks to the high-resolution silicon tracker detector and the high magnetic field of its solenoid. The main CMS recent results on these two topics, the suppression of hard probes and collective flow, are reported here.

3.1 Hard Probes

Jet quenching has been observed in two-jet events, resulting in a significant dijet p_T imbalance in lead-lead collisions. However in dijet events both the leading and sub-leading jets are quenched, therefore it has been suggested to measure this imbalance in photon+jet pairs events, where the photon is not expected to be modified while passing through the medium. The analysis has been performed by CMS in events with pairs of an isolated photon and a jet, comparing PbPb and pp collisions at $\sqrt{s} = 5.2$ TeV [19]. Jets are reconstructed with the anti-k_T algorithm and are required to satisfy $p_T > 30$ GeV and $|\eta| < 1.6$; photons are selected with $p_T^\gamma > 40$ GeV. In order to select clean photon+1 jet events, a $\Delta\phi$ separation of $7/8\pi$ is required among the photon and the jet. Figure 9 shows the ratio of the p_T of the jet to the p_T of the photon in lead-lead and pp collisions, in different bins of centrality. The centrality is a degree of the overlap between the two colliding particles and is estimated by the energy in the CMS forward calorimeters, which cover the forward rapidity region of $2.9 < |\eta| < 5.2$. The centrality bins are marked in percentile of the total inelastic cross section, with the most central 30% of the events marked for instance as 0-30% centrality. The figure shows clearly that in lead-lead interactions the ratio decreases as the collision becomes more

PoS(BORMIO2017)042

central, showing that a large fraction of jets loose energy while traversing the medium, while the jets p_T does not vary in the reference pp collisions.

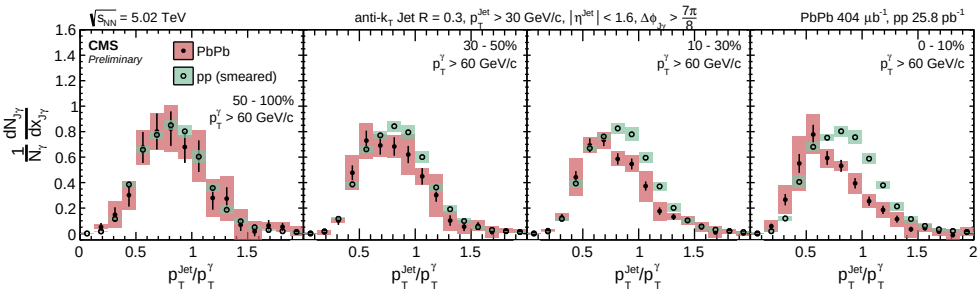

Figure 9: Distribution of the ratio of the p_T of the jet and of the photon in photon+jet pairs of pp and PbPb collisions normalized by the number of photon+jet pairs. The momenta of jets in pp are smeared by the relative jet energy resolution to be used as the reference of each centrality bin. The error bars on the points represent the statistical uncertainty while the shaded coloured boxes represent the systematic uncertainty.

The nuclear modification factor R_{AA} was studied for the first time by CMS for charged particles up to very high p_T at $\sqrt{s} = 5.02$ TeV [20]. The results are shown in Fig. 10 where R_{AA} is shown for primary charged tracks spanning a range in p_T between 0.5 and 400 GeV, and for different centrality values. The suppression of charged particles is of a factor up to 7-8 in the most central collisions and in the p_T range around 6-9 GeV. As the collisions become more peripheral, there is a weakening of the suppression and a weaker p_T dependence. The right figure shows also the equivalent result in pPb, integrated over all centralities, where no suppression is observed.

CMS has also measured for the first time the production of charged B mesons, at $\sqrt{s_{NN}} = 5.02$ TeV [21]. Figure 11 shows the nuclear modification factor R_{AA} measured for B mesons for a p_T range between 7 and 50 GeV. A clear suppression of production of B mesons is seen in lead-lead compared to pp collisions, which results to be of the same order of the one observed for J/ψ mesons (not shown here). The plot also shows the same quantity for D mesons and for charged particles, where the latter are dominated by light quarks. There is no evidence for a dependence on the particle flavour, b, c or uds. However it should be noted that the statistical precision of the data is still limited, and that fragmentation effects are not taken into account. Note also that first top candidate events were observed in the pPb run in 2016 at $\sqrt{s} = 8.16$ TeV.

While there seems to be no evidence for a dependence on the flavour, the study of the charmonium states provides additional important tests on the medium. It is expected that different quarkonium states will dissociate at different temperatures with a suppression dependent on the binding energy: the more weakly-bound states are expected to disappear at temperatures near that of the deconfined QGP phase, T_C, around 150 to 190 MeV. The excited $\psi(2S)$ state has a larger size and a weaker binding energy compared to that of the J/ψ, making it easier for the $\psi(2S)$ to dissociate and melt while traversing the QGP medium. A very useful variable is the double ratio $(N_{\psi(2S)}/N_{J/\psi})_{PbPb}/(N_{\psi(2S)}/N_{J/\psi})_{pp}$, where many systematic uncertainties cancel. The ratio is shown for the CMS data in Fig. 11 [22]. It is less than unity in all p_T bins, implying that the $\psi(2S)$

PoS(BORMIO2017)042

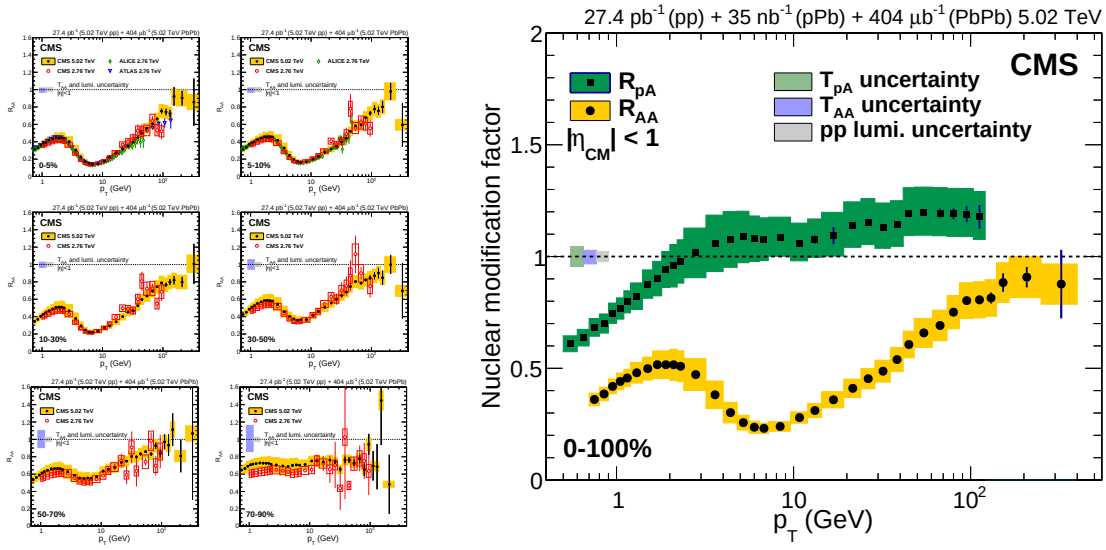

Figure 10: Left: Charged-particle R_{AA} measured in six different centrality ranges and compared also to ALICE and ATLAS data. Right: Measurements of the nuclear modification factor for an inclusive centrality class for both PbPb and pPb collisions. In both plots, the coloured shaded boxes show the CMS systematic uncertainties.

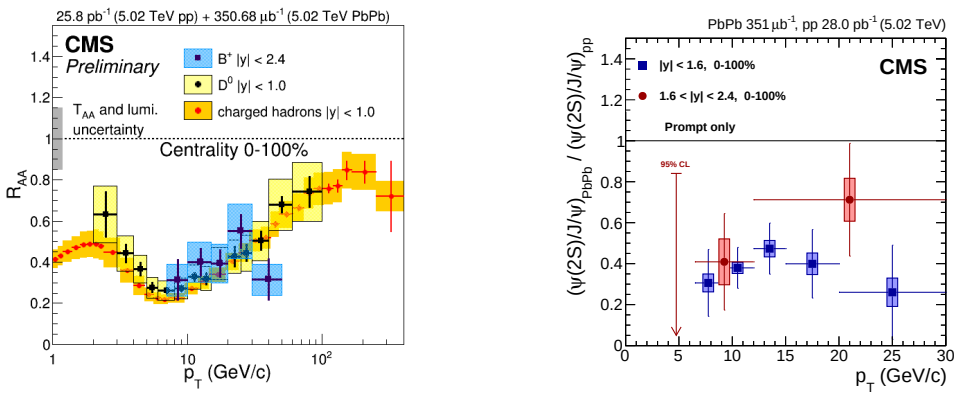

Figure 11: Left: R_{AA} measured for $B^{\pm}$ mesons and compared to the results obtained for D mesons and charged hadrons. Right: Transverse momentum dependence of the double ratio $(N_{\psi(2S)}/N_{J/\psi})_{\mathrm{PbPb}}/(N_{\psi(2S)}/N_{J/\psi})_{\mathrm{pp}}$.

is more suppressed that the J/ψ in PbPb collisions. There is no sign in this transverse momentum range of rigeneration, where the ratio is expected to raise to one.

More dramatic is the suppression in the bottonium family. The $\Upsilon(3S)$ state has one of the lower binding energies, around 200 MeV, and therefore close to the temperature T_C. As it can be clearly seen in Fig. 12, the $\Upsilon(1S)$ and $\Upsilon(2S)$ are more and more suppressed in PbPb compared to pp collisions, while the $\Upsilon(3S)$ seems even to readily melt in the medium.

PoS(BORMIO2017)042

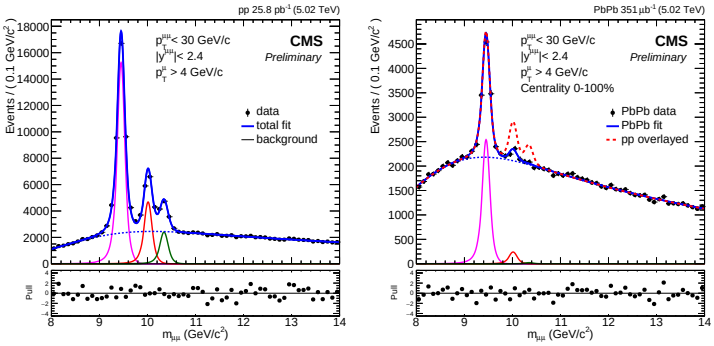

Figure 12: Dimuon invariant mass distributions (black circles) for pp data (left) and centrality-integrated PbPb data (right). The fit is shown as a solid blue line and the background component as a dashed blue line. Υ(1S), Υ(2S), and Υ(3S) are also depicted as solid magenta, red and green lines, respectively. The dashed red line in the PbPb panel represents the pp Υ signal fit normalized at the Υ(1S) mass. The lower panels show the pull distributions.

4. Collective Flow Phenomena

The study of anisotropies in the azimuthal angle distributions of charged particles provide important complementary information to jet quenching. These anisotropies are described by the v_n coefficients of a Fourier expansion in the distributions of azimuthal angle measured with respect to the event plane. CMS has measured the azimuthal anisotropy of charged particles produced in PbPb collisions at $\sqrt{s_{NN}} = 5.02$ TeV for the first time up to very high transverse momenta, $p_T = 100$ GeV [24]. The first two coefficients, the elliptic flow coefficient v_2 describing the elliptical shape of the initial geometry, and the triangular coefficient v_3 describing its fluctuations, are reported in Fig. 13. They are shown for a wide range in p_T and in intervals of centralities. The v_2 and v_3 first increase with p_T up to $\simeq 3$ GeV and then decrease again. The value of v_2 remains positive up to very high $p_T \simeq 70$ GeV, while v_3 remains positive in the central collisions up to $p_T \simeq 20$ GeV.

The 2016 heavy ion pPb run was the last one for a long period, while the next heavy ions run will be in 2018. However higher precision results are coming from the Run 2 2015-2016 data.

Acknowledgments

I would like to thank the organizers for a very nice enjoyable conference and the ATLAS and CMS colleagues who helped me in preparing the talk and proceedings.

References

[1] A. Minaenko, these proceedings.

[2] R. Slovak, these proceedings.

[3] ATLAS Collaboration, *The ATLAS experiment at the CERN Large Hadron Collider*, JINST **3** (2008) S08003.

[4] CMS Collaboration, *The CMS experiment at the CERN LHC*, JINST **3** (2008) S08004.

PoS(BORMIO2017)042

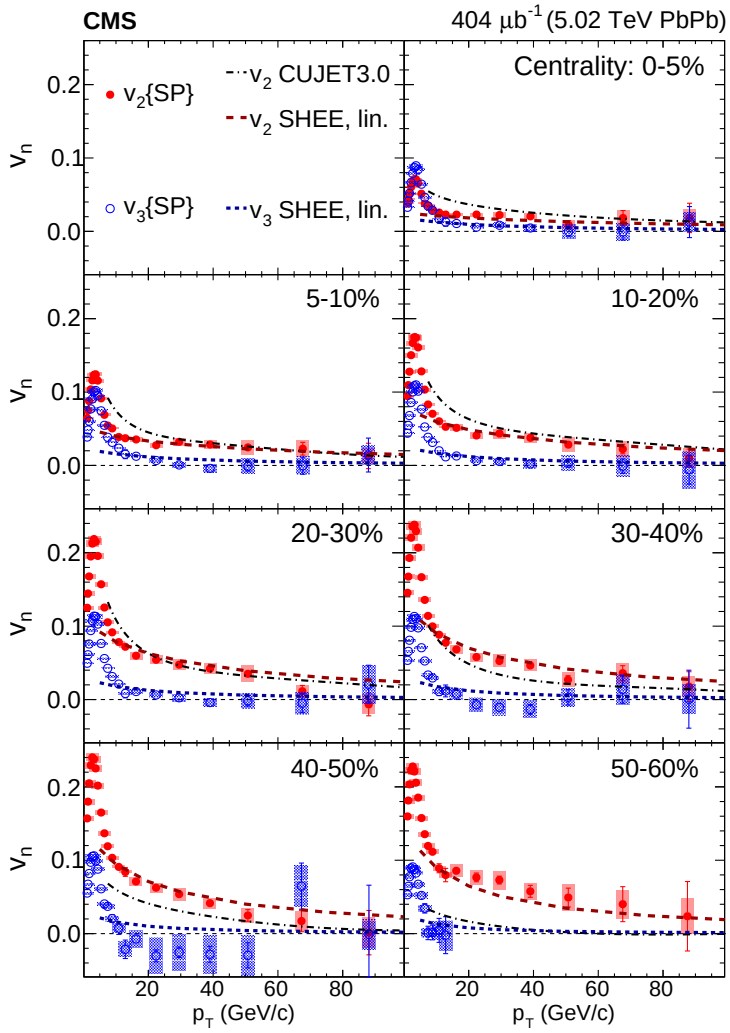

Figure 13: The v_2 and v_3 results, obtained from the scalar product method and as a function of p_T, in seven collision centrality ranges from 0-5% to 50-60%. The vertical bars (shaded boxes) represent the statistical (systematic) uncertainties. The data are compared to two theoretical models. The model calculation (SHEE) incorporating initial-state fluctuations with a linear path-length dependence of parton energy loss is found to be in good agreement with the data.

[5] ATLAS Collaboration, *Precision measurement and interpretation of inclusive W^+, W and Z/γ production cross sections with the ATLAS detector*, arXiv:1612.03016.

[6] ATLAS Collaboration, *Measurement of the W-boson mass in pp collisions at $\sqrt{s}$= 7 TeV with the ATLAS detector*, arXiv:1701.07240.

[7] M. Grazzini et al., *WZ production at hadron colliders in NNLO QCD*, Phys. Lett. **B 761** (2016) 179 [arXiv:1604.08576].

[8] ATLAS Collaboration, *Measurement of the WZ boson pair-production cross section in pp collisions at $\sqrt{s}$ = 13 TeV with the ATLAS Detector*, Phys. Lett. **B 762** (2016) 1 [arXiv:1606.04017].

PoS(BORMIO2017)042

[9] CMS Collaboration, *Measurement of the WZ production cross section in pp collisions at $\sqrt{s}$= 7 and 8 TeV and search for anomalous triple gauge couplings at $\sqrt{s}$= 8 TeV*, arXiv:1606.05721; CMS Collaboration, *Measurement of the WZ production cross section in pp collisions at $\sqrt{s}$= 13 TeV*, Phys. Lett. **B 766** (2017) 268, [arXiv:1607.06943].

[10] ATLAS Collaboration, *Measurement of the ZZ production cross section in pp collisions at $\sqrt{s}$=13 TeV with the ATLAS detector*, Phys. Rev. Lett. **116** (2016) 101801.

[11] CMS Collaboration, *Measurement of the ZZ production cross section and $Z \to l^+ l l'^+ l'^-$ branching fraction in pp collisions at $\sqrt{s} = 13$ TeV*, Phys. Lett. **B 763** (2016) 280 [arXiv:1607.08834].

[12] CMS Collaboration, *Measurement of the $t\bar{t}$ production cross section using events with one lepton and at least one jet in pp collisions at $\sqrt{s}$= 13 TeV*, arXiv:1701.06228.

[13] CMS Collaboration, *Measurement and QCD analysis of double-differential inclusive jet cross sections in pp collisions at $\sqrt{s}$= 8 TeV and ratios to 2.76 and 7 TeV* , JHEP **03** (2017) 156 [arXiv:1609.05331].

[14] S. Catani and M. Grazzini, *An NNLO subtraction formalism in hadron collisions and its application to Higgs boson production at the LHC*, Phys. Rev. Lett. **98** (2007) 222002, [arXiv: hep-ph/0703012].

[15] R. Gavin et al., *FEWZ 2.0: A code for hadronic Z production at next-to-next-to-leading order*, Comput. Phys. Commun. **182** (2011) 2388, [arXiv:1011.3540].

[16] Z. Nagy, *Three-jet cross sections in hadron-hadron collisions at next-to-leading order*, Phys. Rev. Lett. **88** (2002) 122003, [arXiv:hep-ph/0110315].

[17] D. Britzger, K. Rabbertz, F. Stober, and M. Wobisch, *New features in version 2 of the fastNLO project*, (2012) arXiv:1208.3641.

[18] CMS Collaboration, *Observation of Long-Range Near-Side Angular Correlations in Proton-Proton Collisions at the LHC*, JHEP **09** (2010) 091, [arXiv:1009.4122].

[19] CMS Collaboration, *Study of Isolated-Photon + Jet Correlations in PbPb and pp Collisions at $\sqrt{s_{NN}} = 5.02$ TeV*, CMS PAS HIN-16-002.

[20] CMS Collaboration, *Charged-particle nuclear modification factors in PbPb and pPb collisions at $\sqrt{s_{NN}} = 5.02$ TeV*, JHEP **04** (2017) 039, [arXiv:1611.0166].

[21] CMS Collaboration, *Study of B^+ meson production in pp and PbPb collisions at $\sqrt{s_{NN}} = 5.02$ TeV using exclusive hadronic decays*, CMS PAS HIN-16-011.

[22] CMS Collaboration, *Relative modification of prompt $\psi(2S)$ and J/ψ yields from pp to PbPb collisions at $\sqrt{s_{NN}} = 5.02$ TeV*, arXiv:1611.01438.

[23] CMS Collaboration, *Strong suppression of Υ excited states in PbPb collisions at $\sqrt{s_{NN}}$=5.02 TeV*, CMS PAS HIN-16-008.

[24] CMS Collaboration, *Azimuthal anisotropy of charged particles with transverse momentum up to 100 GeV/c in PbPb collisions at $\sqrt{s_{NN}} = 5.02$ TeV*, arXiv:1702.00630.

PoS(BORMIO2017)042